LEAP-Asia-2018 Numerical Simulation Exercise

Zhijian Qiu

Graduate Student Researcher, UC San Diego

Ahmed Elgamal

Professor of Geotechnical Engineering, UC San Diego

Department of Structural Engineering

University of California, San Diego

La Jolla, California 92093-0085

January 9th 2018

CONTENT

FIGURES

1 Soil constitutive model

The employed soil constitutive model (Yang 2000; Elgamal *et al.* 2003; Parra 1996; Yang and Elgamal 2002) were developed based on the multi-surface-plasticity theory (Morz 1967; Iwan 1967; Prevost 1978; Prevost 1985). In this employed soil constitutive model, the shear-strain backbone curve was represented by the hyperbolic relationship with the shear strength based on simple shear (reached at an octahedral shear strain of 10%). The small strain shear modulus under a reference effective confining pressure p'_r is computed using the equation $G = G_0(p'/p'_r)^n$, where p' is effective confining pressure. The dependency of shear modulus on confining pressure is taken as (n = 0.5). The critical state frictional constant M_f (failure surface) is related to the friction angle ϕ (Chen and Mizuno 1990) and defined as M_f = 6sinϕ/(3-sinϕ). As such, the soil is simulated by the implemented OpenSees material PressureDependMultiYield02. Brief descriptions of this soil constitutive model are included below.

1.1 Yield function

The yield function is defined as a conical surface in principal stress space (Prevost 1985, Lacy 1986; Yang and Elgamal 2002):

$$f = \frac{3}{2}\left(\boldsymbol{s} - \left(p' + p'_0\right)\boldsymbol{a}\right) : \left(\boldsymbol{s} - \left(p' + p'_0\right)\boldsymbol{a}\right) - M^2\left(p' + p'_0\right)^2 = 0 \qquad (1)$$

where, $\boldsymbol{s} = \boldsymbol{\sigma}' - p'\boldsymbol{\delta}$ is the deviatoric stress tensor, $\boldsymbol{\sigma}'$ is the effective Cauchy stress tensor, $\boldsymbol{\delta}$ is the second-order identity tensor, p' is mean effective stress, p'_0 is a small positive constant (0.3 kPa in this paper) such that the yield surface size remains finite at $p' = 0$ for numerical convenience and to avoid ambiguity in defining the yield surface normal to the yield surface apex.

$\boldsymbol{\alpha}$ is a second-order deviatoric tensor defining the yield surface center in deviatoric stress subspace, *M* defines the yield surface size, and ":" denotes doubly contracted tensor product.

1.2 Contractive phase

Shear-induced contraction occurs inside the phase transformation (PT) surface ($\eta < \eta_{PT}$), as well as outside ($\eta > \eta_{PT}$) when $\dot{\eta} < 0$, where, η is the stress ratio and η_{PT} is the stress ratio at phase transformation surface. The contraction flow rule is defined as (Yang *et al.* 2003):

$$P" = (1 - \frac{\dot{\boldsymbol{n}}:\dot{\boldsymbol{s}}}{||\dot{\boldsymbol{s}}||}\frac{\eta}{\eta_{PT}})^2(c_1 + c_2\gamma_d)(\frac{p'}{p_a})^{c_3}(c_4 \times CSR)^{c_5} \quad (2)$$

where c_1,-c_5 are non-negative calibration constants, γ_d is octahedral shear strain accumulated during previous dilation phases, p_a is atmospheric pressure for normalization purpose, *CSR* is cyclic stress ratio, and $\dot{\boldsymbol{s}}$ is the deviatoric stress rate. The $\dot{\boldsymbol{n}}$ and $\dot{\boldsymbol{s}}$ tensors are used to account for general 3D loading scenarios, where, $\dot{\boldsymbol{n}}$ is the outer normal to a surface. The parameter c_3 is used to represent the dependence of pore pressure buildup on initial confinement (i.e., K_σ effect).

1.3 Dilative phase

Dilation appears only due to shear loading outside the PT surface ($\eta > \eta_{PT}$ with $\dot{\eta} > 0$), and is defined as (Yang *et al.* 2003):

$$P" = (1 - \frac{\dot{\boldsymbol{n}}:\dot{\boldsymbol{s}}}{||\dot{\boldsymbol{s}}||}\frac{\eta}{\eta_{PT}})^2 d_1(\gamma_d)^{d_2}(\frac{p'}{p_a})^{-d_3} \quad (3)$$

where d_1, d_2 and d_3 are non-negative calibration constants, and γ_d is the octahedral shear strain accumulated during all dilation phases in the same direction as long as there is no significant who wrote this load reversal. It should be mentioned that γ_d accumulates even if there are small unload-

reload phases, resulting in increasingly stronger dilation tendency and reduced rate of shear strain accumulation.

1.4 Neutral phase

When the stress state approaches the PT surface ($\eta = \eta_{PT}$) from below, a significant amount of permanent shear strain may accumulate prior to dilation, with minimal changes in shear stress and p' (implying $p" = 0$). For simplicity, $P" = 0$ is maintained during this highly yielded phase until a boundary defined in deviatoric strain space is reached, and then dilation begins. This yield domain will enlarge or translate depending on load history (Yang *et al.* 2003).

Table 1.1 Sand Model Parameters.

Model Parameters	*Dr.* = 50%	*Dr.* = 60%
Reference mean effective pressure, p'_r (kPa)	101.0	101.0
Mass density, ρ (t/m^3)	2.0	2.02
Maximum shear strain at reference pressure, $\gamma_{max,r}$	0.1	0.1
Shear modulus at reference pressure, G_r (MPa)	100.0	150.0
Stiffness dependence coefficient d, $G = G_r(\frac{\boldsymbol{P'}}{\boldsymbol{P'_r}})^{\boldsymbol{d}}$	0.5	0.5
Poisson's ratio v for dynamics	0.4	0.4
Shear strength at zero confinement, c (kPa)	0.3	0.3
Friction angle ϕ, with resulting shear strength defined as $p' \sin\phi$	44°	44°
Phase transformation angle, ϕ_{PT}	36°	36°
Contraction coefficient, c_1	0.1	0.1
Contraction coefficient, c_2	50.0	20.0
Contraction coefficient, c_3	0.15	0.15
Contraction coefficient, c_4	5.5	5.6
Contraction coefficient, c_5	4.9	5.0
Dilation coefficient, d_1	0.06	0.08
Dilation coefficient, d_2	3.0	3.0
Dilation coefficient, d_3	0.15	0.15
Damage parameter, Liq_1	0.6	0.6
Damage parameter, Liq_2	0.0	0.0
Permeability (m/s)	10^{-5}	10^{-5}

2 Cyclic Torsional Shear Test for *Dr* = 50%

2.1 Cyclic number of cycles for liquefaction

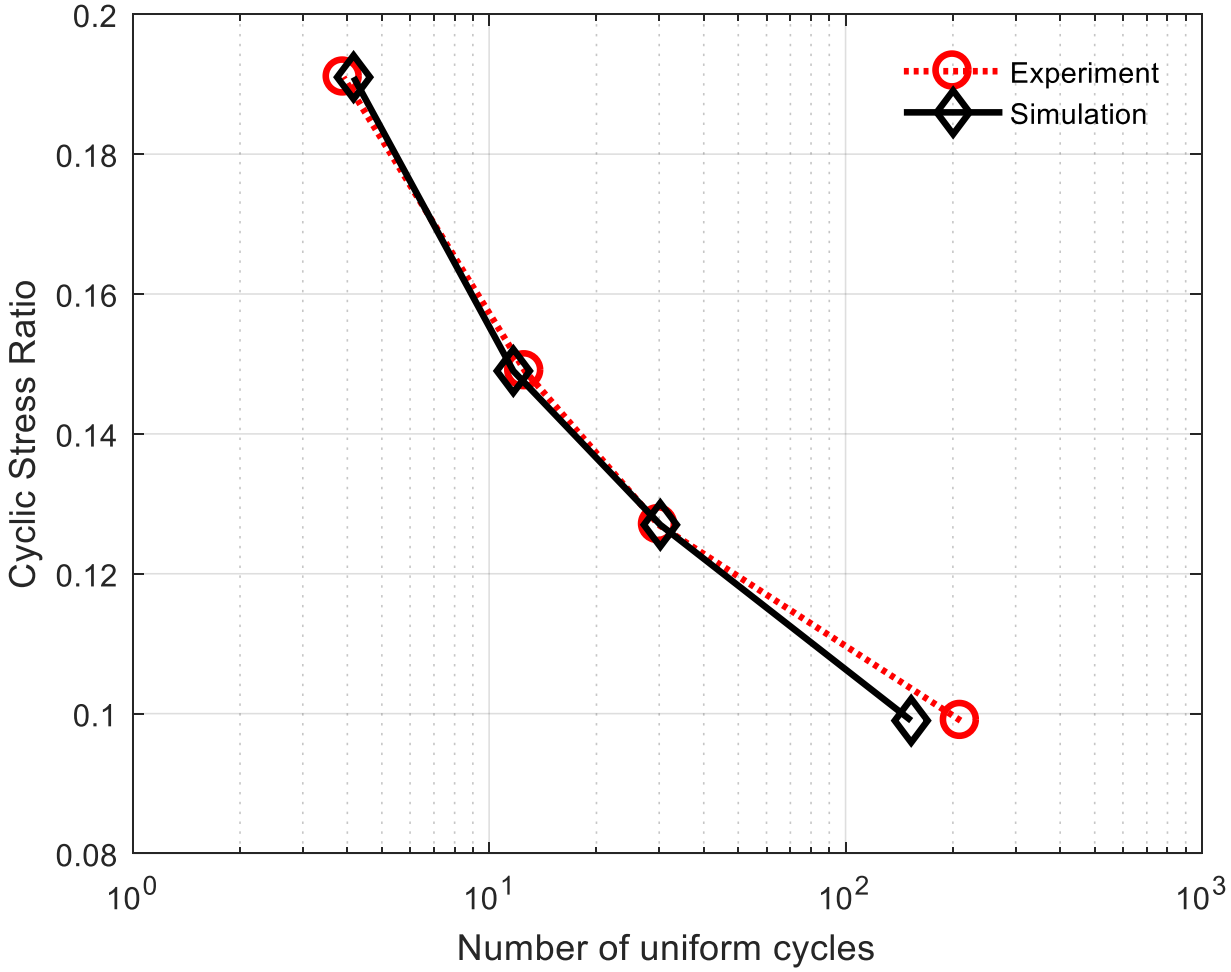

Figure 2.1 Cyclic number of cycles for liquefaction.

2.2 Cyclic stress ratio = 0.191

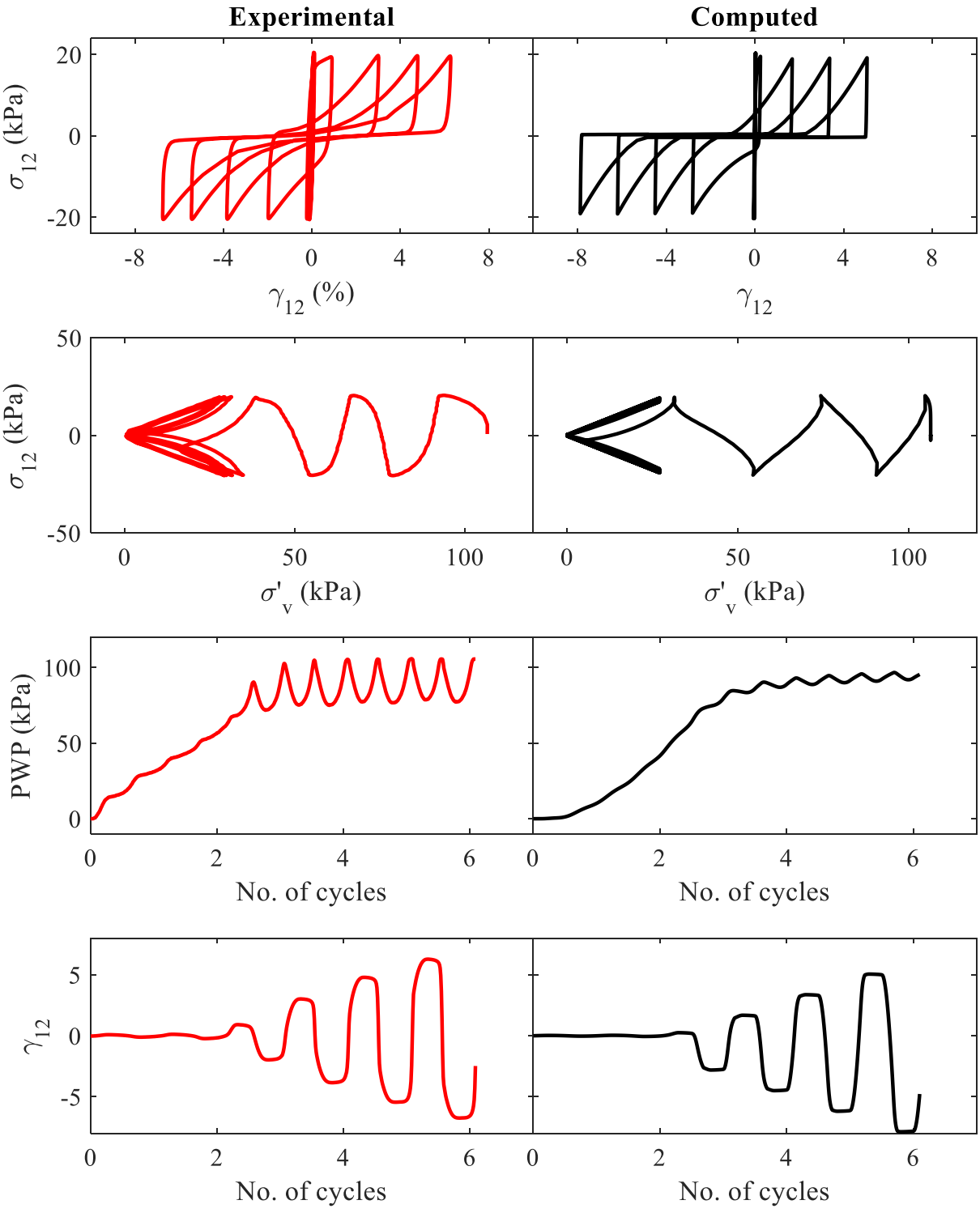

Figure 2.2 Computed and laboratory results for CSR = 0.191.

2.3 Cyclic stress ratio = 0.149

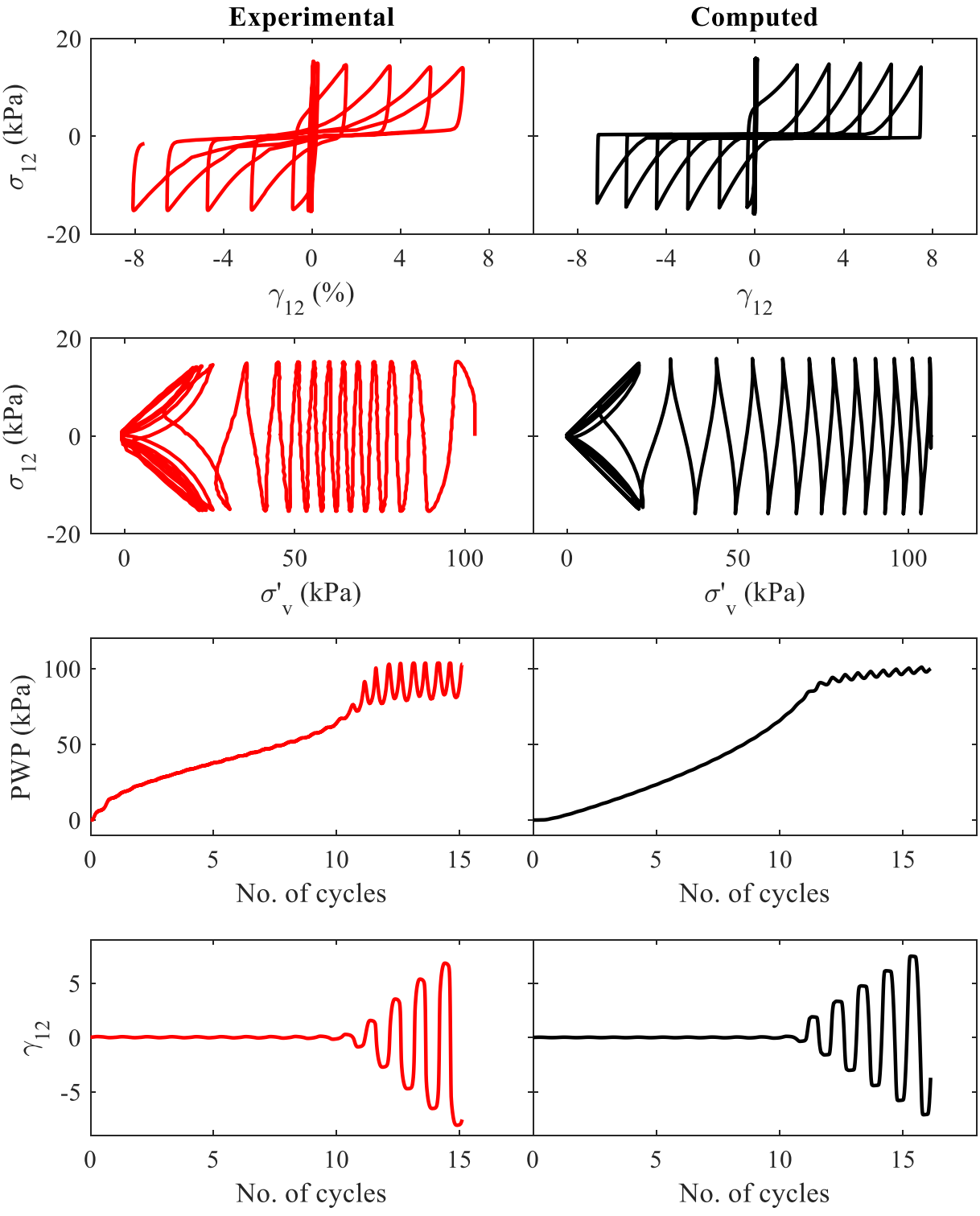

Figure 2.3 Computed and laboratory results for CSR = 0.149.

2.4 Cyclic stress ratio = 0.127

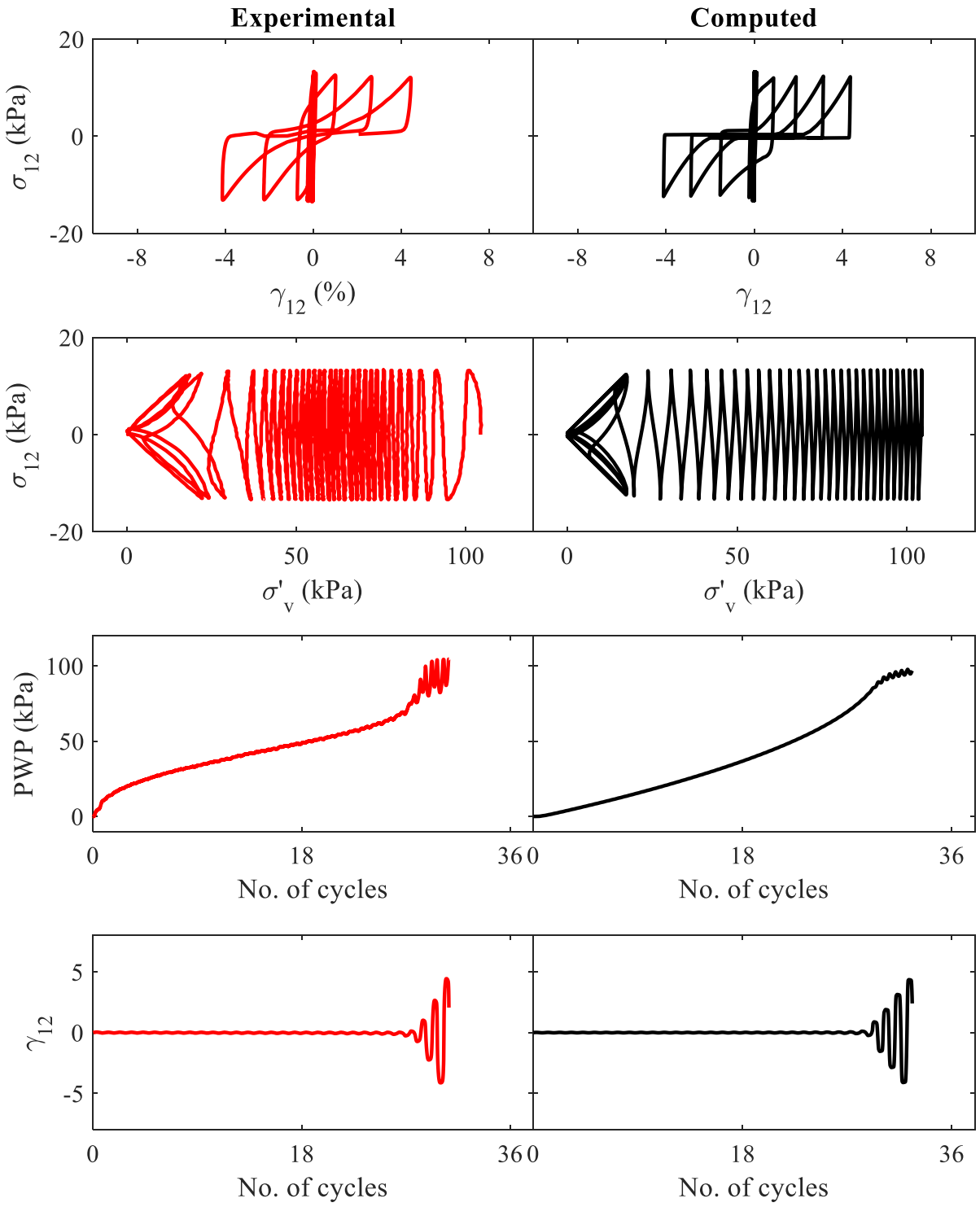

Figure 2.4 Computed and laboratory results for CSR = 0.127.

2.5 Cyclic stress ratio = 0.099

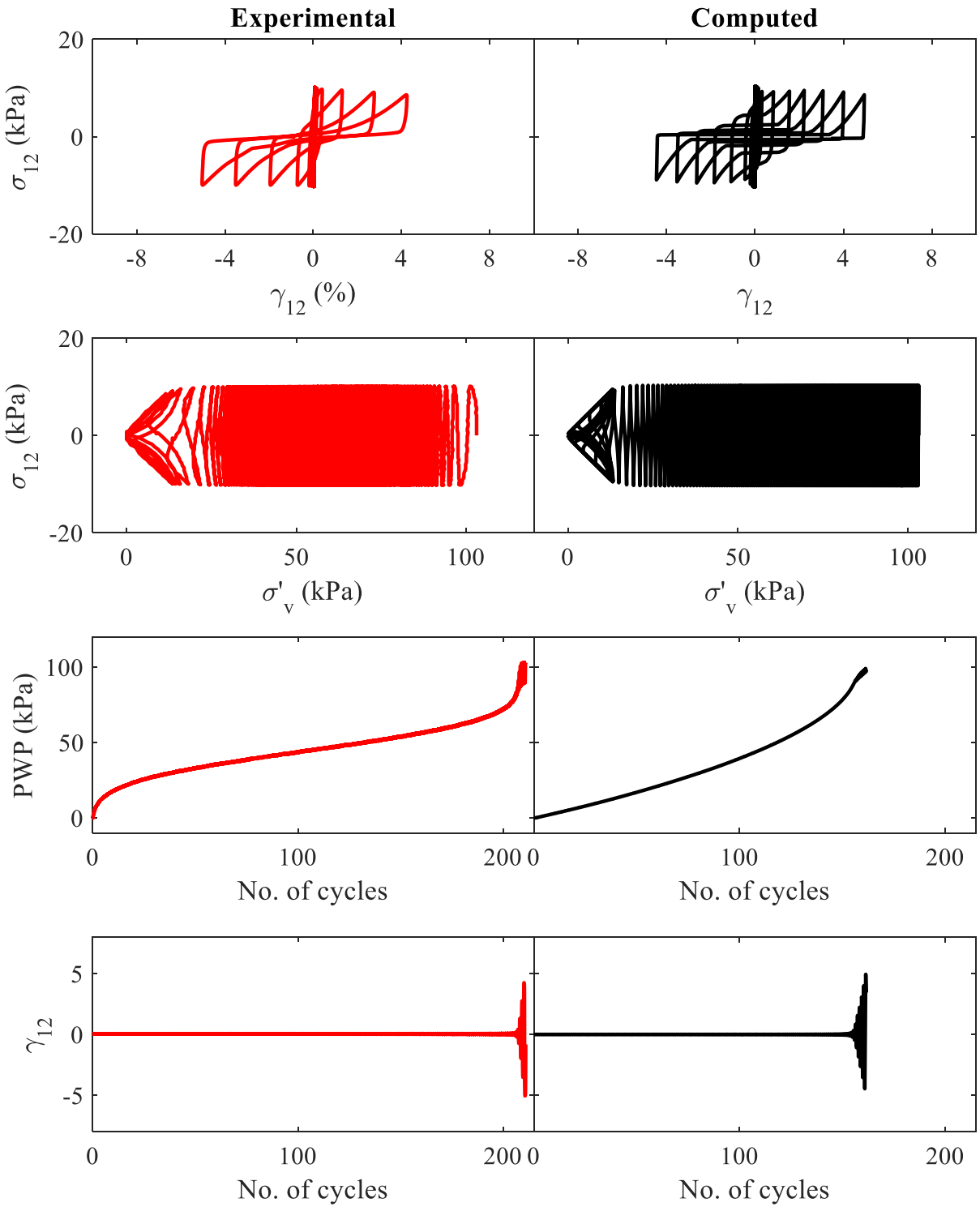

Figure 2.5 Computed and laboratory results for CSR = 0.099.

3 Cyclic Torsional Shear Test for *Dr* = 60%

3.1 Cyclic number of cycles for liquefaction

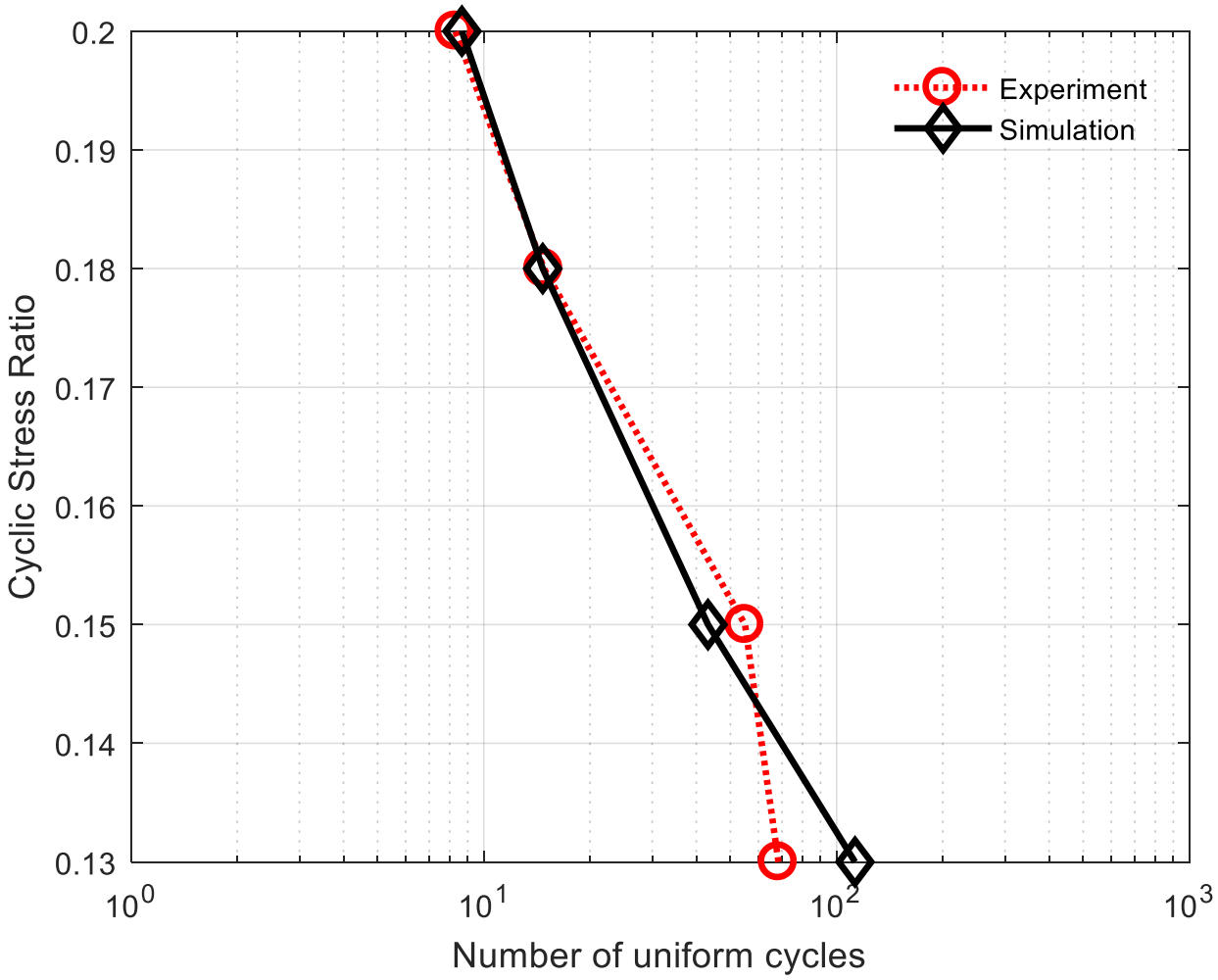

Figure 3.1 Cyclic number of cycles for liquefaction.

3.2 Cyclic stress ratio = 0.2

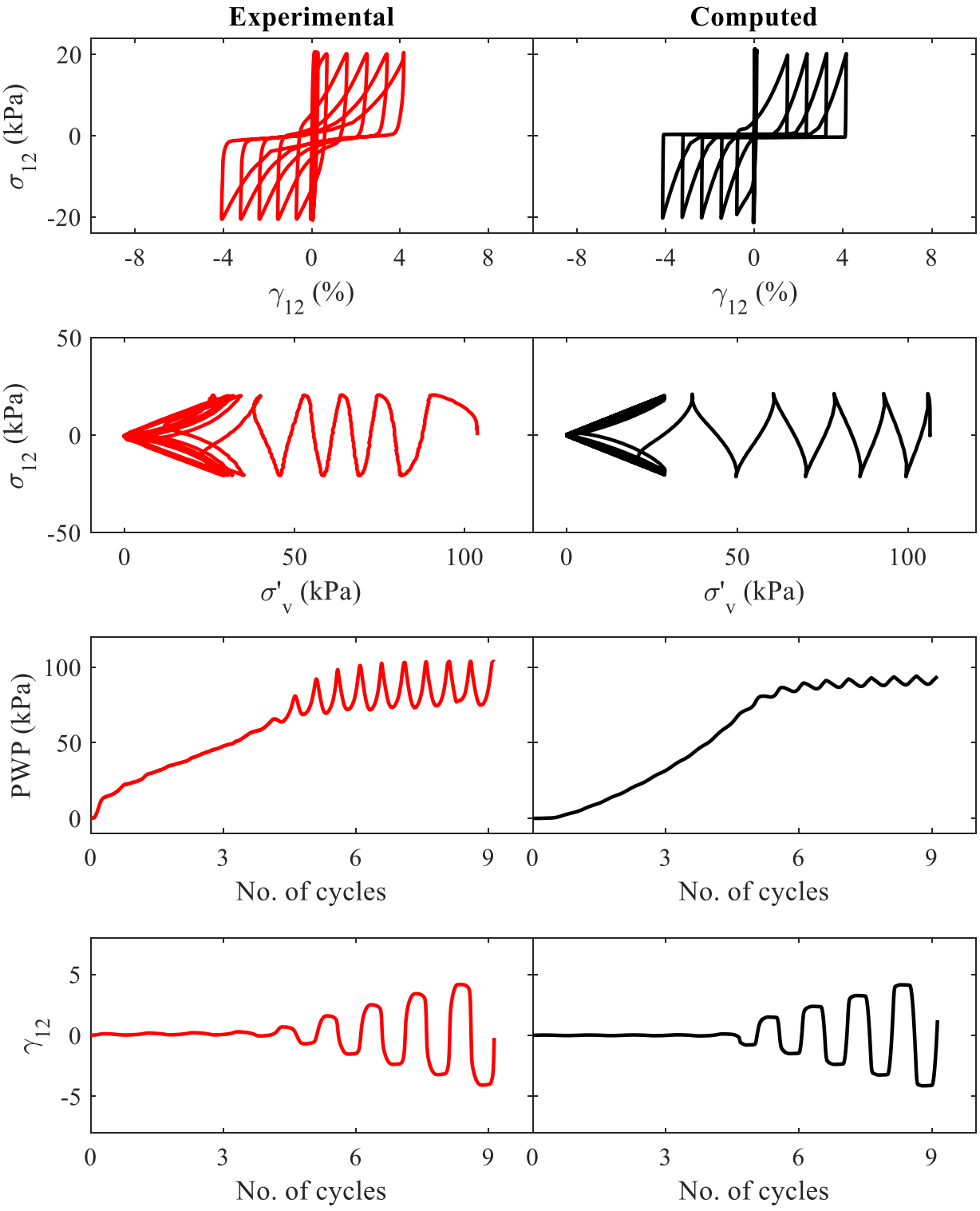

Figure 3.2 Computed and laboratory results for CSR = 0.2.

3.3 Cyclic stress ratio = 0.18

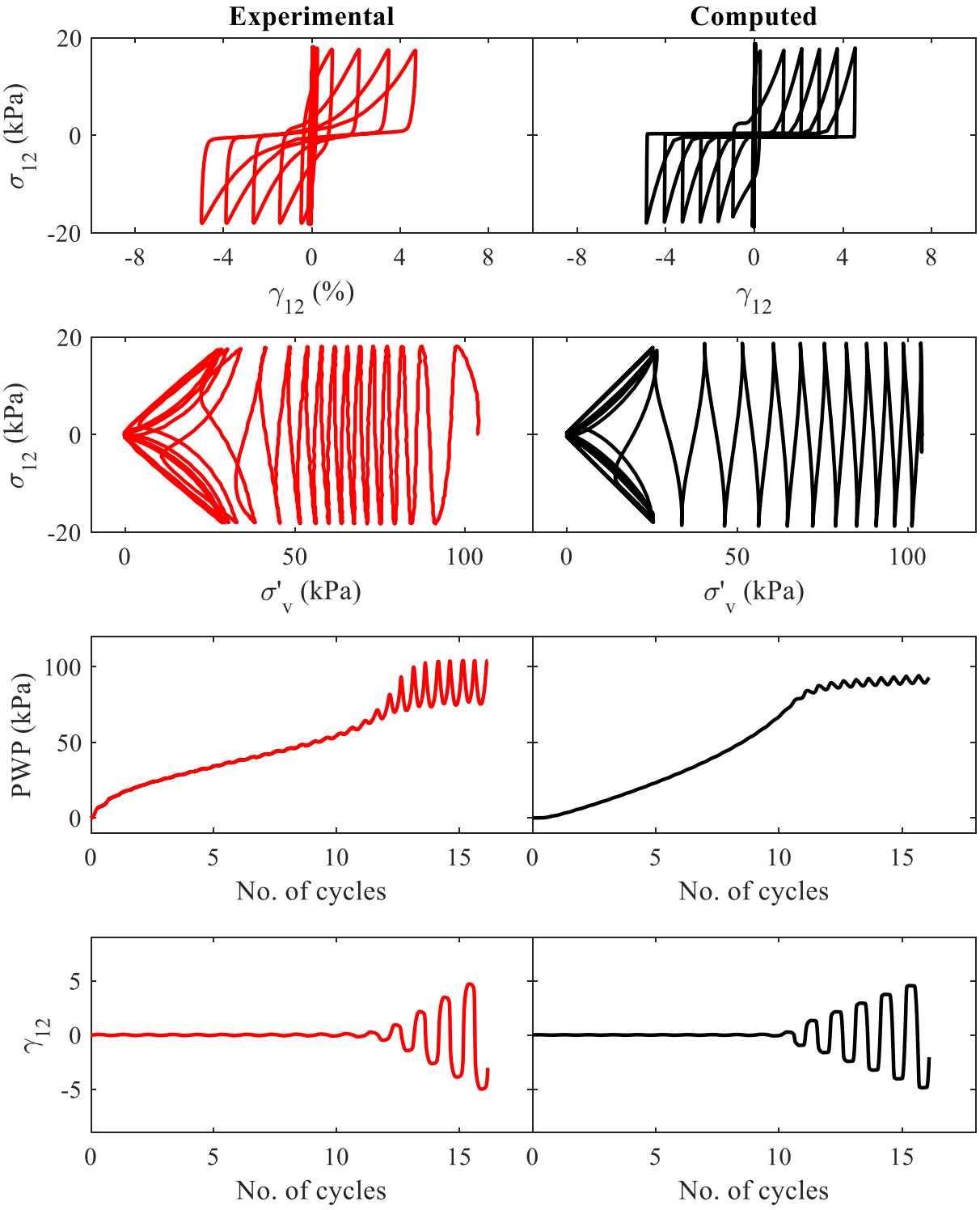

Figure 3.3 Computed and laboratory results for CSR = 0.18.

3.4 Cyclic stress ratio = 0.15

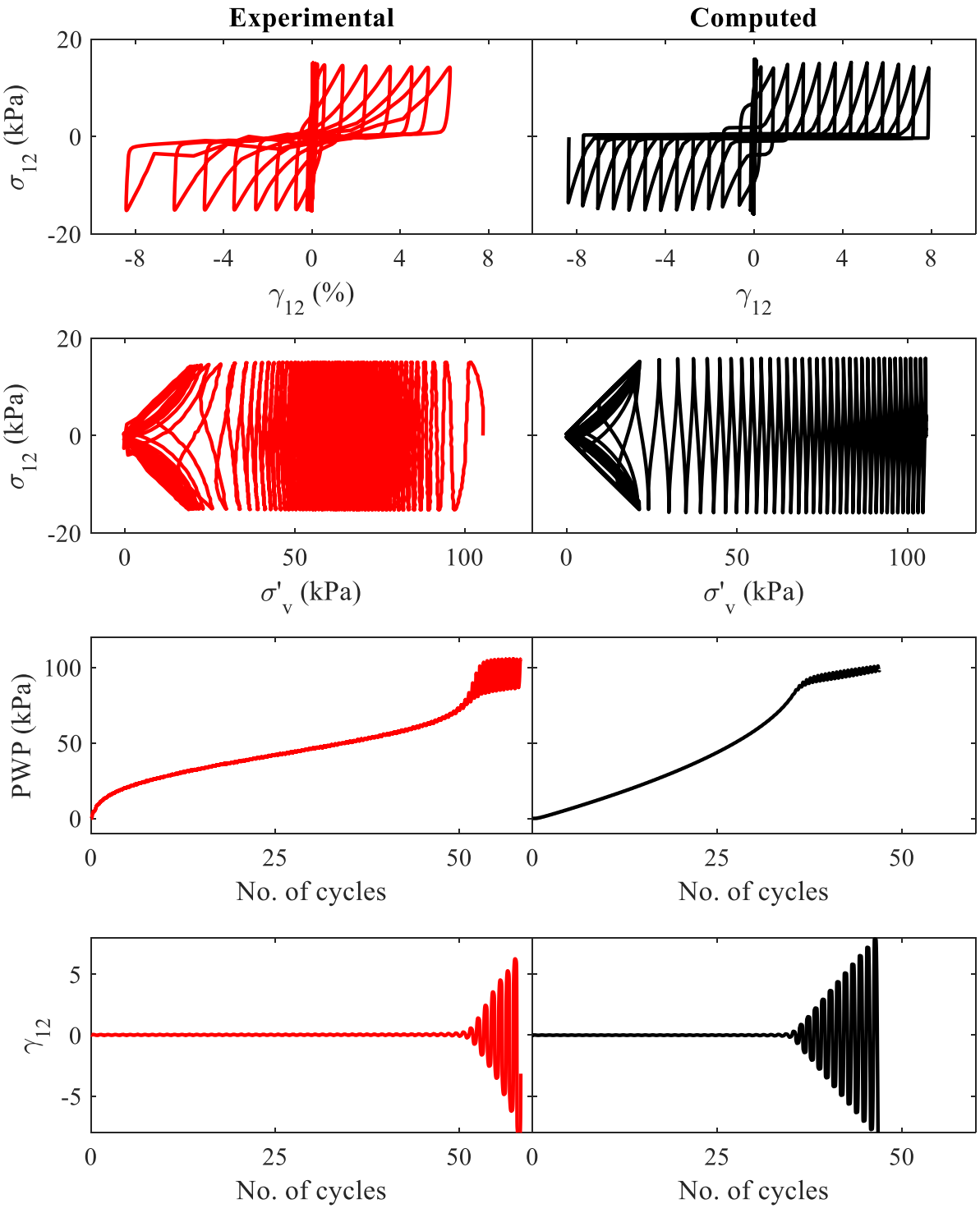

Figure 3.4 Computed and laboratory results for CSR = 0.15.

3.5 Cyclic stress ratio = 0.13

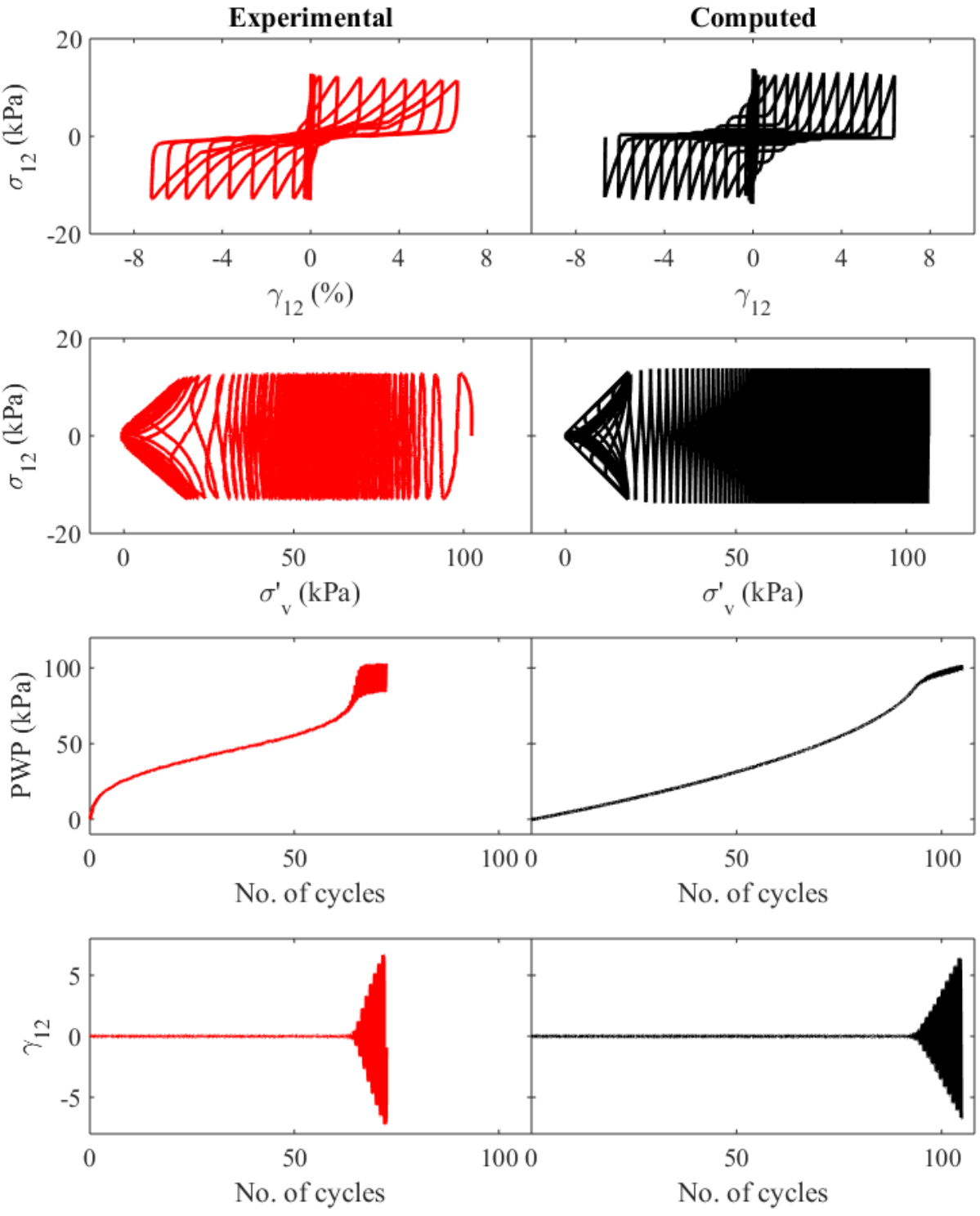

Figure 3.5 Computed and laboratory results for CSR = 0.13.

References

Chen, W.F. and Mizuno, E. (1990). Nonlinear Analysis in Soil Mechanics, Theory and Implementation, Elsevier, New York, NY.

Elgamal A., Yang Z., and Parra E. (2003). "Modeling of cyclic mobility in saturated cohesionless soils." *International Journal of Plasticity*, 19(6), 883-905.

Iwan, W.D. (1967). "On a class of models for the yielding behavior of continuous and composite systems." *Journal of Applied Mechanics*, ASME, 34, 612-617.

Lacy, S. (1986). "Numerical Procedures for Nonlinear Transient Analysis of Two-phase Soil System." *Ph.D. dissertation*, Princeton University, New Jersey.

Mroz, Z. (1967). "On the description of anisotropic work hardening." *Journal of the Mechanics and Physics of Solids*, 15(3): 163-175.

Parra E. (1996). "Numerical modeling of liquefaction and lateral ground deformation including cyclic mobility and dilation response in soil systems." PhD Thesis. Rensselaer Polytechnic Institute.

Prevost J.H. (1978). "Plasticity theory for soil stress-strain behavior." *Journal of the Engineering Mechanics Division*, 104(5), 1177-1194.

Prevost J.H. (1985). "A simple plasticity theory for frictional cohesionless soils." *Soil Dynamics and Earthquake Engineering*, 4(1), 9-17.

Yang Z. (2000). "Numerical modeling of earthquake site response including dilation and liquefaction." PhD Thesis, Columbia University.

Yang Z., and Elgamal A. (2002). “Influence of permeability on liquefaction-induced shear deformation.” *Journal of Engineering Mechanics*, 128(7): 720-729.

Yang, Z., Elgamal, A. and Parra, E. (2003). “Computational model for cyclic mobility and associated shear deformation. Journal of Geotechnical and Geoenvironmental Engineering.” 129(12), 1119-1127.